Rheological Properties of Wet Soils and Clays under Steady and Oscillatory Stresses

Teamrat A. Ghezzehei and Dani Or*

ABSTRACT

Tilled agricultural soils are in a constant state of change induced by variations in soil strength due to wetting and drying and compaction by farm implements. Changes in soil structure affect many hydraulic and transport properties; hence their quantification is critical for accurate hydrological and environmental modeling. This study highlights the role of soil rheology in determining time-dependent stress–strain relationships that are essential for prediction and analysis of structural changes in soils. The primary objectives of this study were (i) to extend a previously proposed aggregate-pair model to prediction of compaction under external steady or transient stresses and (ii) to provide experimentally determined rheological information for the above models. Rheological properties of soils and clay minerals were measured with a rotational rheometer with parallel-plate sensors. These measurements, under controlled steady shear stress application, have shown that wet soils have viscoplastic behavior with well-defined yield stress and nearly constant plastic viscosity. In contrast, rapid transient loading (e.g., passage of a tractor) is often too short for complete viscous dissipation of applied stress, resulting in an elastic (recoverable) component of deformation (viscoelastic behavior). Measured viscoelastic properties were expressed by complex viscosity and shear modulus whose components denote viscous energy dissipation, and energy storage (elastic). Results show that for low water contents and fast loading (tractor speed), the elastic component of deformation increases, whereas with higher water contents, viscosity and shear modulus decrease. Steady and oscillatory stress application to an aggregate pair model illustrates potential use of rheological properties towards obtaining predictions of strains in soils.

Soil compaction by externally applied stresses and internal capillary tension results in soil structure modifications that are of wide interest because of the influence of such changes on transport processes, root growth, and soil mechanical strength. Soil deformation involves time-dependent reorientation and displacement of constituents at microscopic and macroscopic levels, and it is commonly characterized by the relative deformation or strain. For agricultural and environmental applications soil strain at pore scale is important [e.g., in the study of evolution of hydraulic properties (Or et al., 2000)], while for geotechnical applications, overall strain and strength properties of the bulk soil are required. Fundamental concepts of soil rheology, which describe the flow behavior of wet soils, are useful for mathematical description of the time-dependent stress–strain relationships under various loading conditions (Mitchell, 1993; Vyalov, 1986).

Soil strain is relatively large and nonuniformly distributed in space and time and is not easily predictable from a given form and magnitude of stress (Hillel, 1998). In engineering soil mechanics, it is very common to determine stress–strain relationship of soils (under equilibrium conditions) empirically from simultaneous measurements of stress and strain, assuming a certain rheological model applies to the particular soil deformation. For example, theory of elasticity is used in Terzaghi's theory of one-dimensional soil consolidation (Taylor, 1948); and the theory of viscoelasticity is applied for study of creep phenomena in soils (McMurdie, 1963). Although very few stress–strain measurements have been carried out at the so-called tillage range in agricultural soils, because of the inherent difficulty of obtaining measurements under field conditions (Keller, 1970), the above empirical methods are often applied for agricultural soil mechanics with little modification (Koolen, 1983). The use of empirical stress–strain relationships for study of soil deformation, especially for agricultural soil mechanics, has several weaknesses. Primarily, the method is not useful for a priori prediction of magnitude and mode of strain (Hillel, 1998). Secondly, the approach is based on equilibrium state stress–strain relations, while deformations in agricultural soils rarely reach equilibrium (Or, 1996), especially when transient and rapid loading by agricultural machinery is considered. Finally, the method is applicable only for describing bulk volume changes, but it cannot be used to explain pore-scale evolutionary processes that are very crucial in flow and transport processes.

A viable alternative approach that circumvents these limitations is to develop pore-scale mechanistic models that are coupled with intrinsic soil rheological properties. Recently, we proposed energy balance–based formulations that provide predictions of soil deformation rates, at pore and bulk scales, induced by capillary forces of water by considering nonequilibrium stress–strain rate relations (Ghezzehei and Or, 2000; Or et al., 2000). These models address soil deformation induced by internal capillary forces, where there is no particularly favored stress direction. This omnidirectional stress is quite different from external stresses that possess strong directionality; usually vertical stresses are higher than horizontal stresses. Moreover, stresses induced by moving farm implements (e.g., tractor passage) have short loading duration. As this study shows, there is a fundamental difference between soil deformation by farm implements (oscillatory stress) and capillary induced strains (steady stress) rooted in the inherent soil properties, manifested in the form of frequency-dependent rheological properties. Hence, the motivation for this study was twofold: (i) to provide independently measured rheological properties for the capillary-induced

Teamrat A. Ghezzehei and Dani Or, Dep. of Plants, Soils and Biometeorology, Utah State Univ., Logan, UT 84322. Received 27 July 2000. *Corresponding author (dani@mendel.usu.edu).

Published in Soil Sci. Soc. Am. J. 65:624–637 (2001).

Abbreviations: CR, controlled shear rate; CS, controlled stress; OSC, sinusoidal (oscillatory) shear stress.

deformation models and (ii) to provide insights into strain rates in externally loaded soils and the required rheological properties. Special emphasis is given to transient loading by farm implements that involve more complex types of strains.

The primary objective of this study was characterization of soil rheological properties at several water content values and different stress conditions. The specific objectives were (i) to provide rheological properties of selected soils and clay minerals, and measurement guidelines for soil characterization; (ii) to qualitatively correlate the observed properties with microscopic properties of clay–water systems; (iii) to demonstrate the potential applications of soil rheological data for prediction of strain conditions under external stresses (e.g., passage of farm implements).

THEORY

The theoretical section is organized as follows: first, basic rheological concepts are reviewed briefly, with special emphasis on stress–strain conditions that exist in soils. Physico-chemical aspects of soil rheology at microscopic and molecular scales are discussed subsequently. Finally, a simplified model of soil aggregates, used to demonstrate potential applications of the rheological properties under different stress conditions, is presented.

Rheological Concepts

Classical mechanics deals with idealized objects, for example, perfect solids, fluids, or plastics. An ideal Hookean (elastic) solid deforms instantaneously when subjected to stress, and the energy invested in deforming the solid is fully stored. When the stress is removed, the original shape is restored (deformation vanishes), while the energy is recovered in full. The extent of elastic strain is linearly related to the stress applied

$$\tau = G\gamma \qquad [1]$$

where τ is tangential shearing stress, γ is shear strain, and the constant of proportionality, G, is shear modulus. The stress–strain relationship of an ideal elastic is shown graphically in Fig. 1a, by the straight line passing through the origin and, mechanically, is analogous to a perfect spring.

An ideal Newtonian fluid is characterized by the resistance of its elemental particles to motion with respect to one another, and the energy invested in deforming viscous material is dissipated entirely. Newtonian flow is induced by any shear stress greater than zero, and progresses at constant velocity (shearing rate), $\dot{\gamma} = d\gamma/dt$ = constant, which is directly proportional to the stress (τ). The rheological equation of state of a Newtonian fluid is given by

$$\tau = \eta\dot{\gamma} \qquad [2]$$

where the constant of proportionality, η, is coefficient of viscosity. In Fig. 1b, the straight line passing through the origin represents the behavior of ideal viscous fluid, and its mechanical analog is a perfect dashpot.

In a perfectly plastic body, deformation can be initiated only when the tangential (shear) stress attains a critical stress value τ_y, called the yield stress. The yield stress is also the maximum stress that can be set in a prefect plastic material. The equation of state for perfectly plastic material is given by

$$\tau_{max} = \tau_y = \text{constant} \qquad [3]$$

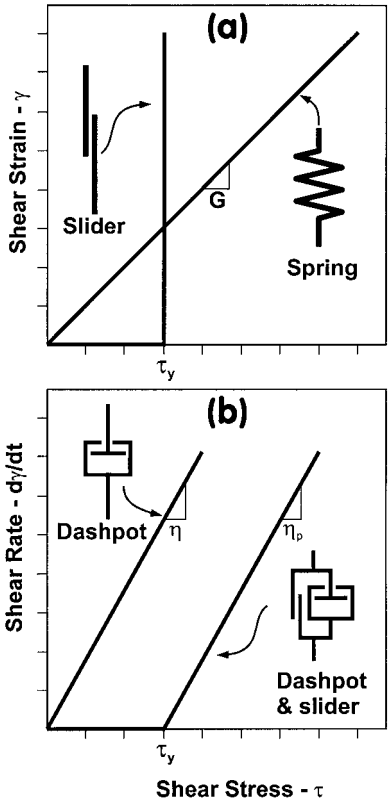

Fig. 1. Rheological curves of ideal materials: (*a*) Stress–strain relations of ideal Hookean solid and flow curve of ideal plastic material with distinct yield stress (τ_y). Spring and slider are mechanical analogs of ideal elastic and plastic solids, respectively. (*b*) Flow curves of ideal Newtonian fluid and Bingham viscoplastic body, and their respective mechanical analogs, dashpot and dashpot-slider.

In Fig. 1a, an ideal plastic material is shown by the curve of zero-strain below the yield stress (τ_y) and vertical line (constant stress) beyond yielding, and the slider is an ideal mechanical analog of perfect plastic material.

Many real bodies, including soil, exhibit mixed behaviors of elasticity, viscosity, and plasticity. For better physical understanding of the equations of state of real materials, it is sometimes easier to visualize them in terms of combinations of analogous mechanical systems (e.g., springs, dashpots, or sliders). In the following subsections, soil rheological properties under two important deformation processes and their mechanical analogs will be discussed.

Soil Deformation under Steady State Stress

Reduction of porosity in wet soil aggregates subjected to steady-state stresses involves welding at interaggregate contact area (Kwaad and Mücher, 1994). Micrographic study of aggregate welding process indicates that flow of soil is initiated only when the stress acting upon the interaggregate contact exceeds a critical yielding point (Day and Holmgren, 1952; McMurdie and Day, 1958). Beyond the yield stress, soil aggregates flow in a manner similar to viscous material at a rate proportional to the stress in excess of the yield stress (Ghavami et al., 1974; Keller, 1970). This combination of plastic and viscous behaviors is commonly referred to as viscoplasticity.

Upon close examination of experimental stress–strain rate relationships of several soils, Vyalov (1986) concluded that a simple linear model of viscoplasticity, the Bingham rheological model, can describe soil deformation under steady-state stress. The equations of flow of Bingham body are given by

$$\dot{\gamma} = 0, \qquad \tau < \tau_y \qquad [4a]$$

$$\dot{\gamma} = \frac{\tau - \tau_y}{\eta_p}, \quad \tau \geq \tau_y \qquad [4b]$$

The coefficient of proportionality, η_p, is analogous to Newtonian viscosity and is commonly referred to as the coefficient of plastic viscosity (Vyalov, 1986). Graphical representation of Bingham viscoplastic material is shown in Fig. 1b by the shifted viscous curve. Mechanical analog of Bingham viscoplastic material is the parallel arrangement of dashpot and slider.

Soil Deformation under Cyclic Stresses

Unlike steady-state stress, transient stresses (e.g., passage of farm implement) act upon soil for a short duration. For example, rear wheels of a typical tractor operating at 2.2 m s^{-1} (5 mph) apply stress on the soil bed for <0.2 s (Harris, 1971). The amount of input energy that dissipates by viscous flow of soil during the short time of stress application is constrained; thus, part of the energy input is stored in elastic strain. The viscous component of the strain is permanent, while the elastic part is restored when the stress is removed (after the tractor passes). The partitioning of strain to recoverable and nonrecoverable components during transient loading of loessal Luvisol by tractor is illustrated in Fig. 2 (Horn and Baumgartl, 1999). The curves represent location of a reference point, initially located at 100 mm below ground surface. The overall strain path, including viscous and elastic deformations, is represented by the position of the observation point. The strain reaches maximum while the tractor weight is still acting. After the tractor has passed, however, strain that involved viscous flow is sustained permanently, while the remaining portion of strain that involved elastic energy storage is recovered. Note also that similar trends of deformation occur laterally at lower magnitude.

We now consider deformation of ideal materials under cyclic stresses. Experimental setup that can be used to conduct such measurements will be discussed in the Materials and Methods section. Consider a homogeneous sample that is subjected to sinusoidal shearing stress (τ) of angular velocity $\omega = 2\pi f$ (where f is frequency), and stress amplitude τ_o (Fig. 3a),

$$\tau = \tau_o \sin(\omega t) \qquad [5]$$

The oscillatory shearing stress induces periodic shear (strain) and shear rate, which can be written in general form as

$$\gamma = \gamma_o \sin(\omega t + \delta) \qquad [6a]$$

$$\dot{\gamma} = \frac{d\gamma}{dt} = \gamma_o \, \varpi \cos(\omega t + \delta) \qquad [6b]$$

where γ_o, is the strain amplitude. The phase shift angle, δ, sometimes called the mechanical loss angle (Dealy, 1982), is described shortly. The time axis is scaled by the frequency (angular velocity) of loading, and is expressed in units of degrees

$$\varphi = (\omega t)\frac{180}{\pi} \qquad [7]$$

Recall from Eq. [1] and Fig. 1a that shearing stress applied upon purely elastic material results in proportional and instantaneous strain. Therefore, if ideal elastic material is tested under oscillatory stress, the stress function Eq. [5] and the strain function Eq. [6a] must be exactly in phase; hence, the phase shift angle in Eq. [6a] and [6b] vanishes ($\delta = 0°$) (thin line in Fig. 3b). For purely viscous materials, Eq. [2] states that the shearing stress is linearly related to the shearing rate. Then, if the material tested under oscillatory stress is an ideal viscous material, the oscillatory stress function Eq. [5] and the strain rate response Eq. [6b] must be in phase, while the stress and strain are out of phase with $\delta = 90°$ (dashed line in Fig. 3b). In other words, the time dependence of viscous shearing results in peak strain delayed by one-half cycle from the peak stress.

Many natural materials, including soil, exhibit intermediate behavior between ideal elastic solids and ideal viscous fluids (dotted line in Fig. 3b), and the phase shift angle is intermediate ($0° < \delta < 90°$). It is more convenient and compact to represent the complementary viscous and elastic properties (viscoelastic) in a complex plane system, as shown below,

The stress and strain amplitudes (τ_o and γ_o in Eq. [5] and [6a], respectively) can be related by an equation of elasticity similar to Eq. [1]

$$\tau_o = G^*\gamma_o \qquad [8]$$

where $G^* = \sqrt{[(G')^2 + (iG'')^2]}$ is a complex shear modulus. The real component of the modulus $G' = G^*\cos(\delta)$ indicates

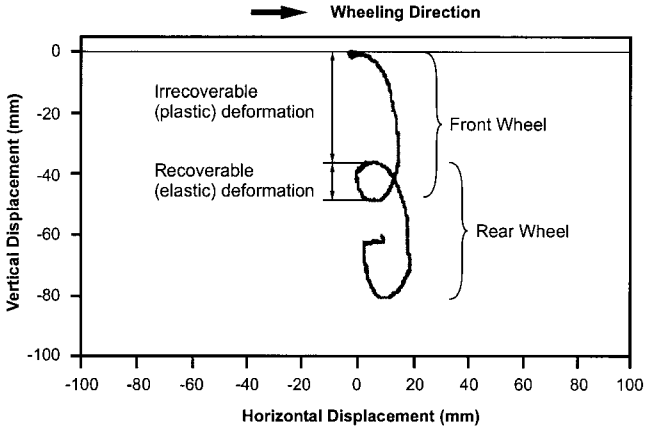

Fig. 2. The loci of observation points, initially 100 mm below the ground surface, during passage of the front and rear wheels of a tractor. Adapted from Horn and Baungartl (1999).

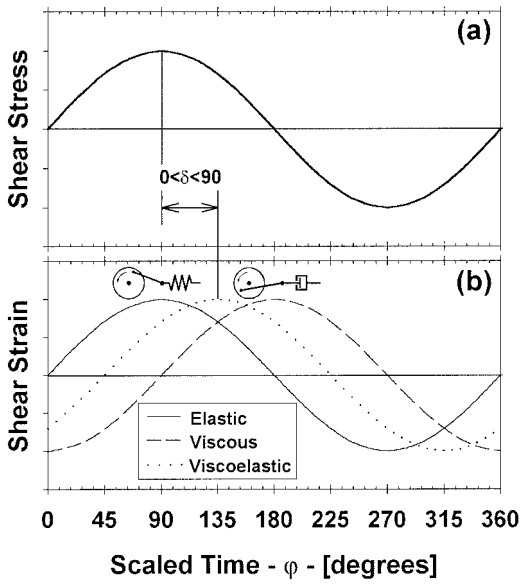

Fig. 3. (*a*) Stress function and (*b*) strain responses of ideal elastic (solid), ideal viscous (dashed), and real viscoelastic (dotted) materials.

storage (elastic) modulus that is related to the recoverable deformation. The imaginary component $G'' = G^*\sin(\delta)$ denotes the loss (viscous) modulus representing the irrecoverable deformation. Note that for perfectly elastic material ($\delta = 0°$), the imaginary component (viscous) vanishes, and the storage (elastic) modulus equals the complex shear modulus. The terms *loss* and *storage* refer to the fact that energy input for deformation dissipates if it is viscous and is stored if it is elastic.

Similarly, the stress and strain rate amplitudes (τ_o and $\gamma_o\omega$ in Eq. [5] and [6b], respectively) can be related by an equation of viscosity similar to Eq. [2]

$$\tau_o = \eta^*\gamma_o\omega \qquad [9]$$

where $\eta^* = \sqrt{[(\eta'')^2 + (i\eta')^2]}$ is complex viscosity. The imaginary component $\eta' = \eta^*\sin(\delta) = G''/\omega$ indicates the loss (dynamic) viscosity and the real component $\eta'' = \eta^*\cos(\delta) = G'/\omega$ denotes storage (elastic) viscosity. For perfectly viscous material ($\delta = 90°$) the real component (storage) vanishes, and the complex viscosity equals the loss viscosity. In summary, the complex viscosity, η^*, (or complex modulus G^*) contains the information necessary for the description of both viscous and elastic strains, and the relative contribution of each is represented by the phase shift angle (δ).

Physico-Chemical Aspects Affecting Soil Rheology

Almost all soil flow and deformation processes evolve from molecular or microscopic interactions (Chenu and Tessier, 1995; Collins and McGown, 1974). Consequently, mechanical processes that govern macroscopic soil rheological properties are determined by arrangement of constituent components and the nature and magnitude of bonds among them (Vyalov, 1986). To facilitate a theoretical discussion pertaining to physical and chemical aspects of soil rheology at microscopic scale, we use a generalized schematic model of a natural soil element, as shown in Fig. 4 (Hueckel, 1992). Assemblage of clay platelets, due to several forms of adhesive forces, creates clay domains (kaolinite) and quasi-crystals (smectite). The domains and quasi-crystals along with silt and fine sand grains, in turn, form microaggregates with an essentially regular network of micropores (intraaggregate pores) filled with liquid water and/or water vapor (Stepkowska, 1990). Because the silt grains are mostly interconnected by clay domains and quasi-crystals (as depicted in Fig. 4) (Collins and McGown, 1974; Dudley, 1970; Mitchell, 1956), mechanical grain–grain interactions are also governed by properties of the clay bridges. The foregoing suggests that soil deformation properties are primarily determined by shearing properties of the clay fraction. Hence, the subsequent brief review of microscopic shearing mechanisms in clay systems will aid in elucidation of macroscopic rheological properties measured in this study.

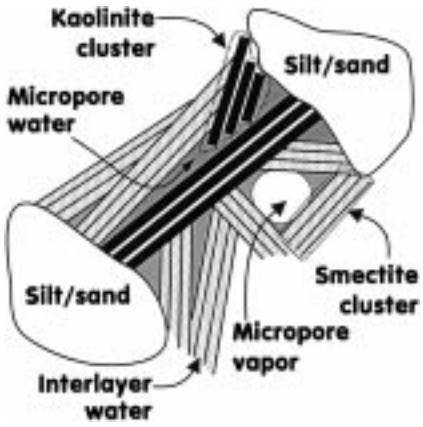

Fig. 4. Schematic model of clay–silt–water system depicting different forms of pore spaces and pore water. Adapted from Hueckel (1992).

Clay minerals are generally classified into two major groups based on the arrangement of their basic unit layers (platelets): expansive and nonexpansive (Chenu and Tessier, 1995). The interlayer spaces of expansive clays (e.g., smectites and vermiculites) can be hydrated; hence, the thickness of these clay minerals is dependent on water content. The extent of permissible expansion is mainly determined by the charge density of the dominant adsorbed cations. In smectites, containing Mg and Ca as exchangeable cations, or containing Na at high salt concentration, the unit clay sheets are closely spaced due to strong electrostatic attraction between the cations and the negatively charged clay surfaces (Keren and Shainberg, 1984). As a result, these smectites have interlayer hydration limited to one to three molecular layers of water, and most of the water contained in the soil is located between clay clusters (as compared with the interlayer space) (Chenu and Tessier, 1995). The close fitting of the water molecules in the interlayer space results in relatively stable structure of the quasi-crystals.

In smectites containing Na, Li, or K in the exchange sites at low salt concentration, the adsorbed ions have large hydration radii and form a wide diffused double layer; thus the electrostatic attraction between clay platelets are weak, forming lose and dispersed tactoids. The interlayer spaces are very expansive and accommodate a large proportion of the total water contained in these clays.

The interlayer spaces of nonexpansive clay minerals (e.g., kaolinite) are anhydrous. Because of the strong interlayer attraction, these minerals have discrete, coarse, and platelike particles (domains) with very high rigidity. The overall physical stability of these clays is very low because of small interparticle (interdomain) contact areas resulting from the rigidity of the particles (Ben-Ohoud and Damme, 1990).

The microrheological properties of clay–water systems are primarily determined by the water content because the weak cohesive forces between water molecules result in yielding to applied stress prior to clay clusters that is, water reduces solid–solid friction by acting as a lubricant. A number of experimental and theoretical studies have shown that water molecules held close to clay surfaces are subject to short- and long-range forces that result in strong ordering and increased viscosity of the molecules relative to their counterparts in bulk state (Israelachvili and Adams, 1978; Schoen et al., 1987). These modifications of liquid behavior are the most likely candidates to describe the macroscopic viscoplastic and viscoelastic properties of clay–water systems.

In experiments by Israelachvili and Adams (1978) two mica surfaces were sheared under different normal forces and with different velocities for a variable number of molecular layers of water. These experiments showed that sliding is initiated after a critical shear stress (yield stress) is reached, similar to plastic materials (see discussions in previous subsection). For a given liquid and clay surface, the yield stress decreased with the number of molecular layers, for example, two molecular layers of water require twice as much stress as required for three molecular layers to shear. Similar trends were reported using water (Kemper, 1964) and nonaqueous liquids (Gee et al., 1990). Numerical simulations of fluids contained between parallel plates, carried out by means of Monte-Carlo and molecular dynamics method (Schoen et al., 1987, 1989; Skipper et al., 1991), showed an abrupt transition of interlayer water from liquid- to solid-type flow by formation of block-like ordered structures when the thickness was reduced to less than six molecular layers. Values of yield stress of bound water from the simulations were similar to experimental.

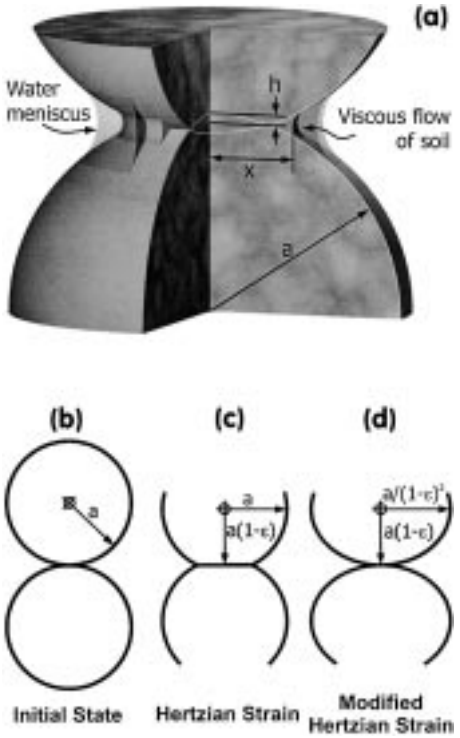

Fig. 5. Aggregate pair model for aggregate coalescence: (*a*) variable definition in viscoplastically strained aggregate pair, (*b*) aggregate pair model before strain, (*c*) aggregate pair model under Hertzian strain, and (*d*) aggregate pair model under modified Hertzian strain.

In summary, adsorption of water molecules onto internal and external clay surfaces of clay minerals induces ordered molecular layering and significant resistance to shearing. The very slow flow (time-dependent) of adsorbed water molecules results in time-dependent viscoelastic behavior of clays at macroscopic scale (Hueckel, 1992). Finite shearing of these ordered molecules occurs only when the stress exceeds a yield point, beyond which the water layers are sheared at higher viscosity that decreases exponentially away from the clay surfaces (Low, 1976; Or and Wraith, 1999) and approaches the properties of the bulk water at about seven to ten molecular layers (Hueckel, 1992).

Apart from the microscopic flow processes of adsorbed water molecules, soil rheological properties at macroscopic scale are further influenced by relative arrangement of clay clusters and silt grains. As the results of this study show, the effect of solid–solid interactions becomes more pronounced with the decrease in thickness of liquid film (water content) separating the solids.

The theory of rate processes (Eyring, 1936; Glastone et al., 1941) has been adapted to describe some aspects of macroscopic, time-dependent soil deformation, and creep phenomena (e.g., Abdel-Hady and Herrin, 1966; Anderslan and Douglas, 1970; Feda, 1989; Mitchell, 1993). The basis of the rate process theory is that movement of flow units (atoms, molecules, or particles) relative to each other is constrained by energy barriers separating adjacent equilibrium positions. Displacement of flow units to new positions requires investing of activation energy sufficient to surmount the barrier, and the deformation process is viewed as sequence of displacements of individual flow units. At any instant, only some of the activated flow units may successfully cross the barrier (signifying viscous flow), while others fall back to their original positions (denoting transient elastic deformation). Although there is no proof that the theory of rate processes describes soil deformation correctly, parts of the theory were successfully tested experimentally (e.g., Feda, 1989; Mitchell et al., 1969).

Simplified Soil Aggregate Model

One of the potential applications of soil rheological measurements is prediction of soil strain deforming under applied steady or cyclic stresses. For illustrative purposes we use a simple model of a pair of equal-sized, spherical aggregates (radius = a), in contact as shown in Fig. 5. The objective of the modeling framework is to predict strain induced to the aggregate pair when subjected to either internal capillary forces or external stresses. The core of the model is equating the net rate of work done by the applied forces to the rate of energy dissipation due to coalescence of wet aggregates. The main factors determining the magnitude and rate of strain are the rheological properties of the soil and the stress conditions. Details of the model and its underlying assumptions for aggregate coalescence under quasi-steady capillary forces (or changing at a slow rate compared with the deformation rate) are given by (Ghezzehei and Or, 2000). In the following, extension of the model for aggregate deformation under external steady and oscillatory stresses will be considered.

Aggregate Coalescence under Steady External Force

The mechanisms governing deformation under external and internal steady stresses are identical. The major difference between the two modes of stresses is steady capillary forces acting upon aggregate pair induce equal stresses in all contacts regardless of their spatial orientation, provided the aggregates have identical geometry and are at equal capillary pressure (Ghezzehei and Or, 2000), while external steady stresses have strong dependence on orientation.

Consider an aggregate pair subjected to a constant external force F, and the aggregates coalesce at their contact while the material forming the contact region flows outward. As a result, the centers of the aggregates move towards the contact plane by h, and the axial strain is given by $\varepsilon = h/a$. The radius (x) of the resulting circular contact area, at time t, can be approximated by

$$x(t)^2 = 2a^2\varepsilon(t) \qquad [10]$$

Then, the axial stress (σ) acting upon the contact area is

$$\sigma(t) = \frac{F}{2\,\pi\,a^2\,\varepsilon(t)} \qquad [11]$$

Because the stress changes at a relatively slow rate, compared to the strain rate, we assume the deformation obeys Bingham law Eq. [4] (i.e., entirely viscoplastic),

$$\sigma(t) = \frac{F}{2\,\pi\,a^2\,\varepsilon(t)} = \lambda_p\left[\frac{d\varepsilon(t)}{dt}\right] + \sigma_y \qquad [12]$$

The coefficient of plastic viscosity in compression [$\lambda_p = 2\eta_p(1 + \upsilon)$ (Vyalov, 1986)] and the yield stress in compression ($\sigma_y = \tau_y/2$) are determined from rheological measurements, where υ is Poisson's ratio. Analytical solution to Eq. [12], subject to the initial condition $\varepsilon(t = 0) = \varepsilon_o$ (initial strain), is given by

$$\varepsilon(t) = \frac{1}{Q}\left\{1 + \text{ProductLog}\left[(Q\varepsilon_o - 1)\exp(Q\varepsilon_o - 1)\exp\left(-\frac{Q\,\sigma_y\,t}{\lambda_p}\right)\right]\right\} \qquad [13]$$

where $Q = (2\pi a^2\sigma_y/F)$. The special function ProductLog(z) = ω is the solution to the nonlinear expression $z = \omega e^{\omega}$ (Abramowitz and Stegun, 1974). In the illustrative examples section, application of Eq. [13] along with viscoplastic-rheological properties of soil will be presented.

Aggregate Deformation under Cyclic Force Application

Unlike the case considered above, where the energy input by external loads has sufficient time to dissipate (via viscous flow), cyclic (transient) loads offer only limited opportunity time for viscous deformation. Hence, part of the energy input that does not dissipate in viscous flow is temporarily stored in elastic deformation. Traditionally, the contact area of two spherical bodies resulting from an entirely elastic deformation is modeled by Hertz theory (Mavko et al., 1998). According to this model, the strain results in only the flattening of the contact areas without affecting large portions of the spheres (Fig. 5c). Considering that flow of soil material at the contact involves viscous dissipation (as discussed above), we propose an alternative energy-conserving mechanism to account for the elastic strain in viscoelastic spheres. We consider elastic deformation of a soil aggregate pair results in bulging of the aggregates without permanent flow (rearrangement) of soil material around the contact (Fig. 5d), with the magnitude of the axial strain being equal to the Hertzian strain. Consequently, when an aggregate pair is subjected to oscillatory stress, the resulting elastic and viscous strains happen at separate locations; that is, the aggregates undergo elastic bulging while the material forming the contacts flows viscously. The elastic deformation is instantaneous while the viscous flow takes place at a rate dictated by wet soil viscosity.

Now, consider a pair of perfectly elastic spheres in contact shown in Fig. 5b; collinear forces are applied so as to press the two spheres together. According to Hertz theory, the elastic spheres deform temporarily at their mutual contact region, forming a circular contact area of radius x (Fig. 5c) given by

$$x = \frac{\sqrt[3]{3}}{2}\left[(1 - \upsilon)\frac{a F}{G}\right]^{1/3} \quad [14]$$

where G is shear modulus of the spheres. An oscillatory input force F (e.g., induced by passage of tractor) may be given by

$$F = F_o\sin(\omega t) \quad [15]$$

Then, the resultant elastic strain (ε_e) at any time t is obtained by substituting Eq. [14] and [15] in Eq. [10]

$$\varepsilon_e(t) = \sqrt[3]{\frac{9}{512}\left(\frac{1 - \upsilon}{a^2 G}\right)^2}\,[F_o \sin(\omega t)]^{2/3} \quad [16]$$

For viscoelastic soils with storage and loss components of elasticity, the storage shear modulus (the real component G' of the complex modulus G^* Eq. [8]) is responsible for the elastic strain Eq. [16]. The resulting Hertzian strain in the pair of spheres is shown schematically in Fig. 5c. For the proposed elastic bulging of soil aggregates (modified Hertzian elastic strain Fig. 5d), the major and minor axes of the resulting ellipsoidal aggregate are obtained from the Hertzian strain by $a(1 - \varepsilon_e)$ and $a/(1 - \varepsilon_e)^2$, respectively.

The deformation (flow) at the interaggregate contact is considered entirely viscous as stated by Eq. [12], without yield stress (i.e. $\sigma_y = 0$). The solution to Eq. [12], with time-dependent input force Eq. [15], is given by

$$\varepsilon_v(t)^2 = \frac{F_o}{2\,\pi^2 a^2 f\lambda'}(1 - \cos[\omega t]) + \varepsilon_o^2 \quad [17]$$

where $\lambda' = 2\eta'(1 + \upsilon)$ is the loss component of the complex viscosity Eq. [9]. The overall axial strain is given by the sum of the elastic Eq. [16] and viscous Eq. [17] components

$$\varepsilon(t) = \varepsilon_e(t) + \varepsilon_v(t) \quad [18]$$

The applications of soil viscoelastic rheological properties and the above models Eq. [18] in solving soil mechanics problems will be demonstrated in the Illustrative Examples section using an example that mimics the effects of fast and slow passage of a tractor.

MATERIALS AND METHODS

Measurement Apparatus

Rheological instruments developed for characterization of other materials (e.g., polymer melts, food materials) have been used for determination of soil properties with some success. For example, rotary viscometers were applied to determine soil plasticity and yield stress of clay mud (Koenigs et al., 1976) and super soft clays (Fakher et al., 1999).

In this study, a rotational (torsional) rheometer with a parallel-plate sensor system (RheoStress RS75, Thermo Haake, Karlsruhe, Germany) was employed. The instrumental setup is shown in Fig. 6. The soil sample is placed between the rotary plate (top) and stationary plate (bottom) at a specified constant spacing (2 mm) between the plates. The shaft of the rotary plate is equipped with sensors that measure torque and angular velocity, and the computerized driver translates them to average shear stress (τ) and shear strain (γ), respectively, using geometrical relations. Two basic alternatives are available to use the above geometry as an absolute rheometer: (i) controlled stress (τ) input and determining the resulting shear rate ($\dot{\gamma}$) (CS mode) or conversely (ii) a controlled shear rate input ($\dot{\gamma}$) and determining the resulting shear stress (τ) (CR mode). When CS- or CR-mode measurements are conducted under steady stress or shear rate applications, respectively, the resulting flow curves can be used to determine viscosity (η or η_p) and yield stress (τ_y) of ideal viscous or viscoplastic materials, as discussed above. The CS- or CR-mode measurements conducted under sinusoidal (oscillatory) shear stress (CS-OSC) or shear rate (CR-OSC) application, respectively, can be used for viscoelastic characterization.

For proper application and interpretation of rheometric test results, the following assumptions must be considered (Dealy, 1982; Thermo Haake, 1994):

1. The shear stress applied must be transmitted fully from the moving plate to the sample (no slippage). Poor cohesion between the steel plate and soil sample can cause substantial slippage at low shear stresses or high water content. Slippage was reduced in our experiments by lining the rheometer plates with fine-grain sandpaper (<0.08 mm) (Banfill and Kitching, 1991).
2. Because soil density and confining pressure are important factors in determining rheology, they should be kept at a constant magnitude to avoid unaccounted variations in the measurement results. For these reasons, the experiments were conducted at constant sample volume (plate–plate spacing of 2 mm) and zero vertical stress.
3. It is assumed that the properties of the test material (soil) have no intrinsic dependence on direction, and the material reacts to applied stress uniformly. Test results

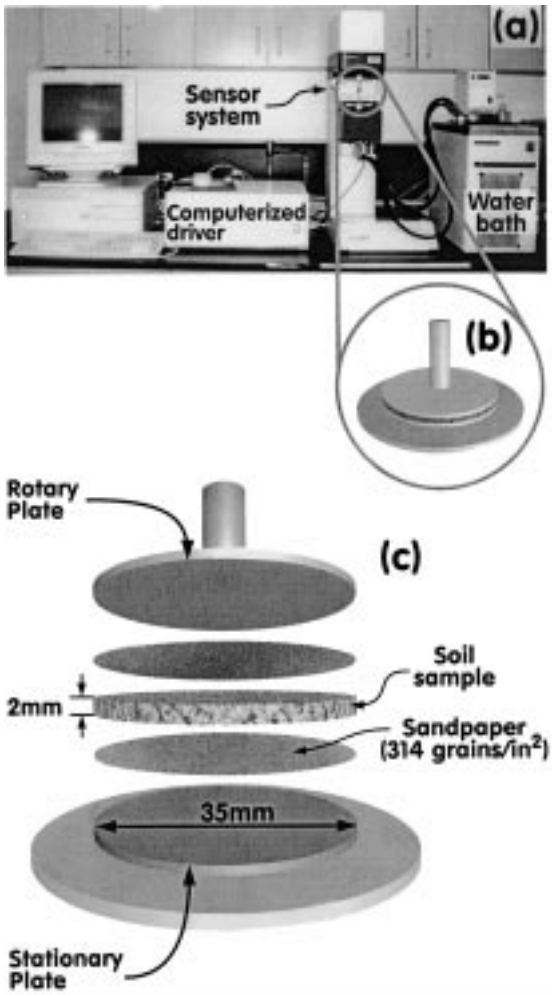

Fig. 6. Rotational rheometer used in this study. (*a*) complete setup, (*b*) sensor system during measurement, and (*c*) arrangement of sand paper and soil sample in sensor system.

reflect average properties of the sample and not of individual flow components.

4. All physical and chemical properties affecting the rheology of the sample must be kept constant during measurement. To reduce loss of soil water by evaporation, the duration of the measurements was limited to 3 to 15 min. The maximum reduction in water content occurred in samples with high water content (2–6 kg kg^{-1}), but was limited to <1%. The temperature of the plates was kept constant by circulating water.

Soils and Clay Minerals Tested

Rheological measurements were conducted on two natural soils [Millville silt loam (coarse-silty, carbonatic, mesic Typic Haploxerolls) and Fraternidad clay soil (fine, smectitic, isohyperthermic Typic Haplusterts)], and three clay minerals (kaolinite, Ca-montmorillonite, and Na-montmorillonite). The rheological properties of the natural soils may be directly linked with processes occurring in agricultural soils. The clay minerals, however, are intended to aid in understanding the fundamental flow behaviors of soil in the absence of heterogeneity and interference by silt and sand fractions. Selected physical and chemical properties of the samples are given in Table 1. The soil samples were sieved through 1.0-mm mesh size. Different water content levels were established for all samples by mixing air-dried soil or clay with an appropriate mass of water and allowing the mixture to equilibrate for 48 to 72 h.

Measurement Procedures

Steady Controlled-Stress Tests

Enough soil or clay samples to fill the 2-mm gap between the parallel plates were placed between the plates. For each sample, new (unused) circular discs of sand paper were affixed to the parallel plates using two-sided adhesive tape, with the rough surface facing the soil. Measurements of stress, strain, and strain rate were conducted at 100 stress points, incremented in logarithmic scale during a total measurement period of 3 min. During pilot tests, two criteria were used in selecting the stress range appropriate for each soil or clay and water content. First, adequate points are required near the yield point for better distinction of the yield stress, and secondly, at the maximum stress (strain rate) the soil sample should remain intact within the plate–plate spacing (at higher strain rate, failure results by high centrifugal forces). At each stress point the computerized driver conducts measurements in triplicate and reports averaged data. The entire procedure was repeated three to five times, for each soil– or clay–water content combination.

Oscillatory Controlled Stress Tests

Sample handling and placement for oscillatory measurement are identical to steady stress measurements. The oscillatory measurements were conducted in the stress range selected for the corresponding steady stress measurements. For every stress point (amplitude τ_o), the stress was applied as full-sine cycle (Fig. 3), and the corresponding strain was recorded. The instrument used has the capability of recording stress and strain values at a resolution of one point for every degree of

Table 1. Selected physical and mineralogical properties of soils (clays) used in this study.

Sample	Source	Texture			Clay composition	Surface area	CEC
		Sand	Silt	Clay			
		%				$m^2\ g^{-1}$	cmol kg^{-1}
Millville silt loam†	Logan, Utah	29	55	16	Kaolinitic + montmorillonitic	73‡	NA
Fraternidad clay§	Lajas Valley, PR	18	31	52	Montmorillonitic	NA	40.5
Kaolin-well ordered	Washington Co, GA	0	0	100	SiO_2 (43.9%); Al_2O_3 (38.5%)	23.5¶	3.3
Ca-montmorillonite	Gonzales Co, TX	0	0	100	SiO_2 (70.1%); Al_2O_3 (16.0%)	83.79¶	84.4
Na-montmorillonite#	Wyoming	0	0	100	Wyoming bentonite (100%)	NA	NA

† Or and Wraith (1999).
‡ EGME method (Carter et al., 1986).
§ Gierbolini (1979).
¶ N_2 method (Olphen and Fripiat, 1979).
# Maycoban Drilling Fluids Services, Dresser Industries, Houston, TX.

scaled time (φ) or better. The phase shift angle (δ) and strain-amplitude (γ_o) were computed from duplicate measurements at each stress point. Because measurements take longer duration at every stress point, only 15 stress increments were used. The frequencies reported in this paper are: 0.0681, 0.6810, and 3.160 Hz.

RESULTS AND DISCUSSION

Viscoplastic Properties of Unsaturated Soil

The steady-state, CS measurements (conducted on the different soil types and water contents) provide relationships of shearing stress (τ) vs. shear strain (γ) and shearing rate ($\dot{\gamma}$). A typical test result for Millville silt loam soil (at 0.28 kg kg^{-1} water content) is depicted in Fig. 7. The stress–strain relationships, plotted in log-log scale (Fig. 7a), are divided into two distinct linear segments. The first segment with a unit slope (in log-log scale) indicates a linear stress–strain relationship. In linear-scale (Fig. 7b), this segment fits a straight line passing through the origin, signifying an elastic deformation regime (Fig. 1a). According to Eq. [1], the inverse slope of the stress–strain function denotes the shear modulus (G). The second linear segment of Fig. 7a, with a slope of above unity (in log-log scale), indicates a linear relationship between the derivative of the strain (strain-rate) and stress (Fig. 7c), and suggests a viscous flow (see Fig. 1b). In line with Eq. [4b], the inverse slope of the stress vs. strain-rate relationship represents the coefficient of plastic viscosity (η_p) of the soil sample. The stress at which transition from the elastic to the viscous segment occurs indicates yielding of the soil sample (yield stress τ_y). One can also notice higher non-linear strain-rate beyond the viscous range, where the sample could not be contained between the plates (failure). In summary, viscoplastic soil flow behavior for a given water content can be described by three parameters: shear modulus (G), yield stress (τ_y), and coefficient of plastic viscosity (η_p).

Viscoplastic parameters of the different soils and clay minerals are shown in Fig. 8. Discussions on effects of stress magnitude, water content, and clay mineralogy on viscoplastic parameters are given below.

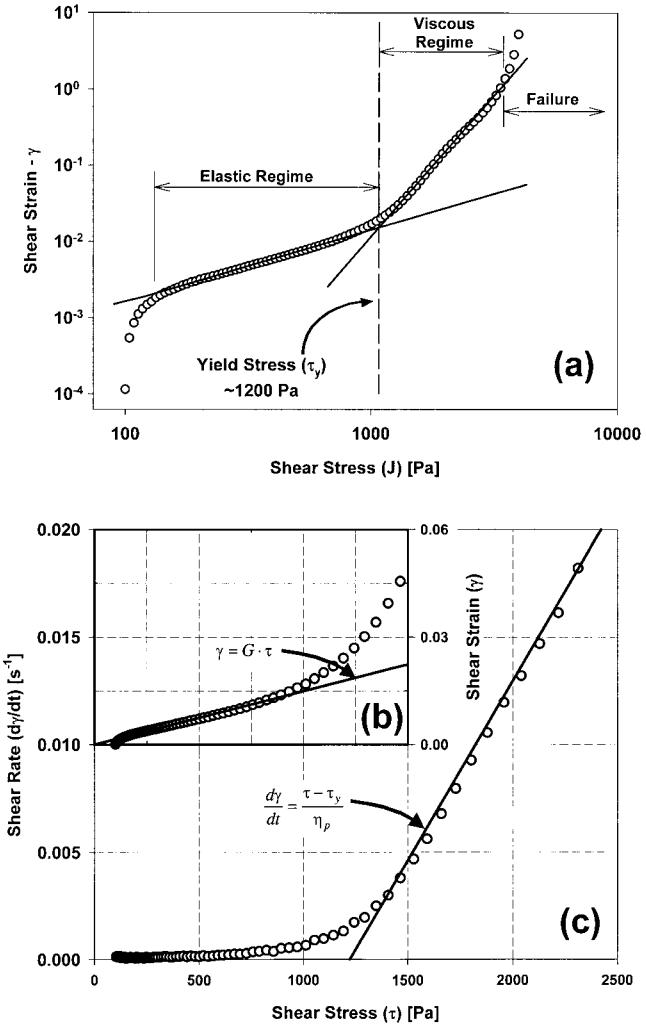

Fig. 7. Typical measurement results for steady state CS measurement (Millville silt loam soil at 0.28 kg kg^{-1} water content). (*a*) Stress–strain relation in log-log scale, showing the distinct differentiation of the deformation to elastic and viscous types; (*b*) elastic range in linear scale; and (*c*) viscous range in linear stress–strain rate curve (flow curve), and definition of Bingham model.

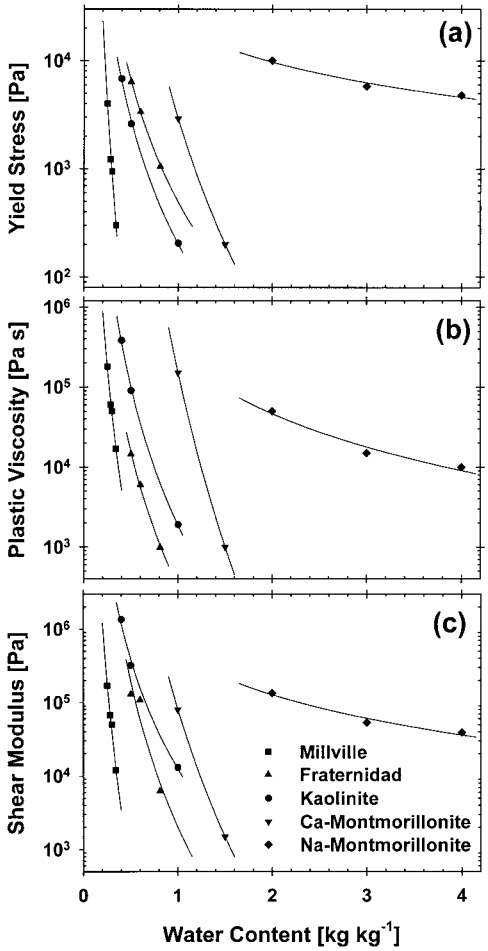

Fig. 8. Viscoplastic parameters of different soil and clay types as function of water content by weight. (*a*) Yield stress, (*b*) coefficient of plastic viscosity and, (*c*) shear modulus. Each point in the plots denotes mean of three to six independent replicates.

The Effect of Stress Magnitude

The division of the flow behavior into elastic and viscous regimes (as shown in Fig. 7a) is typical for all the soils and clay tested. Low applied stress can be accommodated with small and temporary bending of solid matrix or stretching of bonds between water molecules without substantial rearrangement of water molecules adsorbed on surfaces of clay domains and quasi-crystals. If the stress is relieved, the strain usually recovers fully. Yielding of the soil and subsequent viscous flow are initiated when temporary bond stretching or bending can no longer accommodate the applied stress. In terms of rate processes theory, the elastic regime is where the energy imposed on an average flow element is insufficient to surmount an energy barrier, hence the deformation is temporary and fully recoverable. Viscous deformation (flow) commences when the stress magnitude reaches a point where it can cause a jump over the energy barrier of an average flow unit.

The Effect of Water Content

Experiments of molecular shearing of water held between mica surfaces (Israelachvili and Adams, 1978) have shown that the tightly adsorbed water molecules have yield stress that is independent of shear rate. Furthermore, they have shown that the viscosity of one or two molecular layers of water is five to seven orders of magnitude higher than the viscosity of bulk water. These findings were in qualitative agreement with soil viscoplastic properties observed in this study, as detailed below.

A decrease in water content is accompanied by an exponential increase in yield stress, shear modulus and viscosity of all the soils tested (Fig. 8), principally due to a decrease in the number of water molecular layers coating clay domains and quasi-crystals, and reduced mobility of the molecules. In addition, decrease in water content leads to reduction of the intergranular spacing. This, in turn, may set off additional resistance to deformation by the enhanced solid–solid interactions.

To further elaborate the effects of water content on viscoplastic properties, properties of Na-montmorillonite clay were determined for a wider water content range (Fig. 9). The yield stress of the clay (Fig. 9a) decreased exponentially with water content. This observation is in agreement with the plastic flow behavior of adsorbed water molecules (Israelachvili and Adams, 1978). In contrast, there was an abrupt reduction in viscosity of the clay by about three orders of magnitude (Fig. 9b) when the water content was increased to more than 6 kg kg^{-1}, signifying a macroscopic transition from solid-like to liquid-like behavior. The main reason for this phenomenon could be that solid-like flow at lower water content is dictated by the shearing of water held between clusters and quasi-crystals, whereas liquid-like flow at higher water content is governed by the flow of liquid in micropores.

The Effect of Clay Type

The effect of clay type is directly related to the specific surface area, activity, and type of adsorbed cations. In general, the larger the internal surface area the larger the liquid mass required to form one molecular layer of water. Consequently, the change in viscoplastic properties with increasing water content is more gradual for Na-montmorillonite than Ca-montmorillonite and kaolinite, as shown in Fig. 8. Although the internal surface area of Ca-montmorillonite is equivalent to that of Na-montmorillonite, the maximum amount of water that can be held in internal surfaces of Ca-montmorillonite is limited to one to three molecular layers. The internal surfaces of kaolinite are practically nonwettable. Hence, large proportion of soil water in Ca-montmorillonite and kaolinite clays is held in intercluster

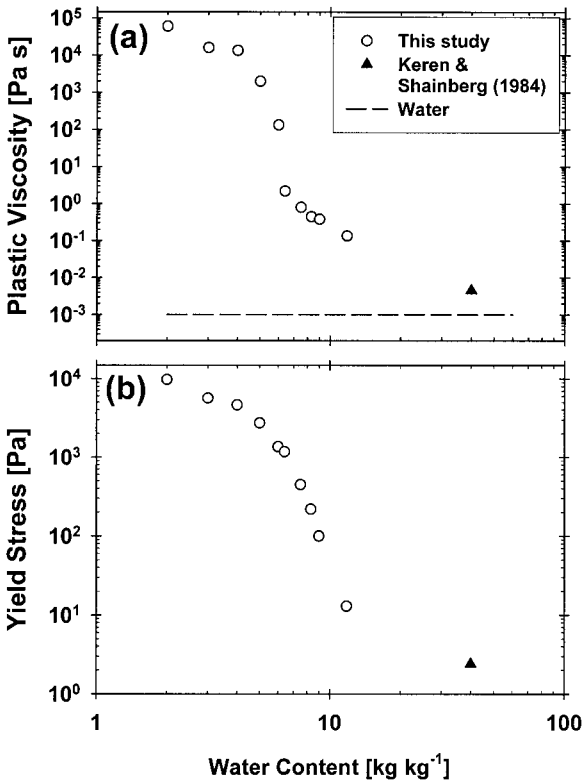

Fig. 9. Viscoplastic parameters of Na-montmorillonite over expanded water content range. (*a*) coefficient of plastic viscosity and (*b*) yield stress. Each point in the plots denotes mean of three independent replicates.

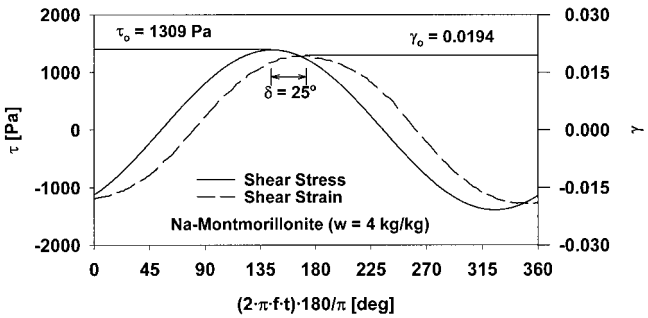

Fig. 10. Typical measurement results of controlled stress oscillatory test of Na-montmorillonite at frequency of 3.16 Hz and water content of 4 kg kg^{-1}.

spaces, resulting in localization of the effective stress in few intercluster contacts. These contacts primarily determine the viscoplastic properties of the clay. This also explains why the viscoplastic properties of both Ca-montmorillonite and kaolinite change with water content at the similar rates. However, the Ca-montmorillonite curve is shifted to the right in Fig. 8 (more wet) because the large quantity of water held in internal surfaces of Ca-montmorillonite does not play as significant a role as the water held between clusters in the rheological properties. The same reasons also explain the shifting of Fraternidad curves (higher surface area) to the right with respect to the Millville curves (lower surface area).

Viscoelastic Properties of Wet Soils and Clay Minerals

Typical measurement output for Na-montmorillonite (water content = 4 kg kg^{-1}) at specified stress-amplitude (τ_o = 1390 Pa) and loading frequency (f = 3.160 Hz) is shown in Fig. 10. The input sinusoidal stress function [$\tau_o \sin(\omega t)$] and resulting strain function are plotted as functions of scaled time φ (Eq. [7]), in the x-axis. All the viscoelastic properties are contained in either the complex viscosity (η^*) or complex modulus (G^*), and the phase shift angle (δ); the remaining parameters can be derived from these (see the Theory section for details).

Summarized viscoelastic properties (complex viscosity η^* and phase shift angle δ) for Millville silt loam soil, Fraternidad clay soil, kaolinite, and Na-montmorillonite are presented in Fig. 11 and 12. The effects of stress magnitude, clay or soil type, water content, and loading frequency on viscoelastic parameters are discussed below.

The Effect of Stress Magnitude

During steady loading, elastic deformation and viscous flow occur under different stress magnitudes (see Fig. 7). During cyclic loading, however, both elastic and viscous deformations occur concurrently at any given stress. The primary reason is that short loading duration offered by oscillatory stress limits the viscous flow and allows for elastic strain–relaxation to take place.

Considering the heterogeneity within a soil sample, at any given stress magnitude, part of the microscopic flow units (e.g., water molecules held between clay clusters and quasi-crystals) may be below their yielding point, whereas others are under viscous state. Moreover, increasing stress magnitude would increase the proportion of the flow units that are under viscous state. Thus, two important consequences of increasing stress can be noted for all the soils or clays and water contents tested

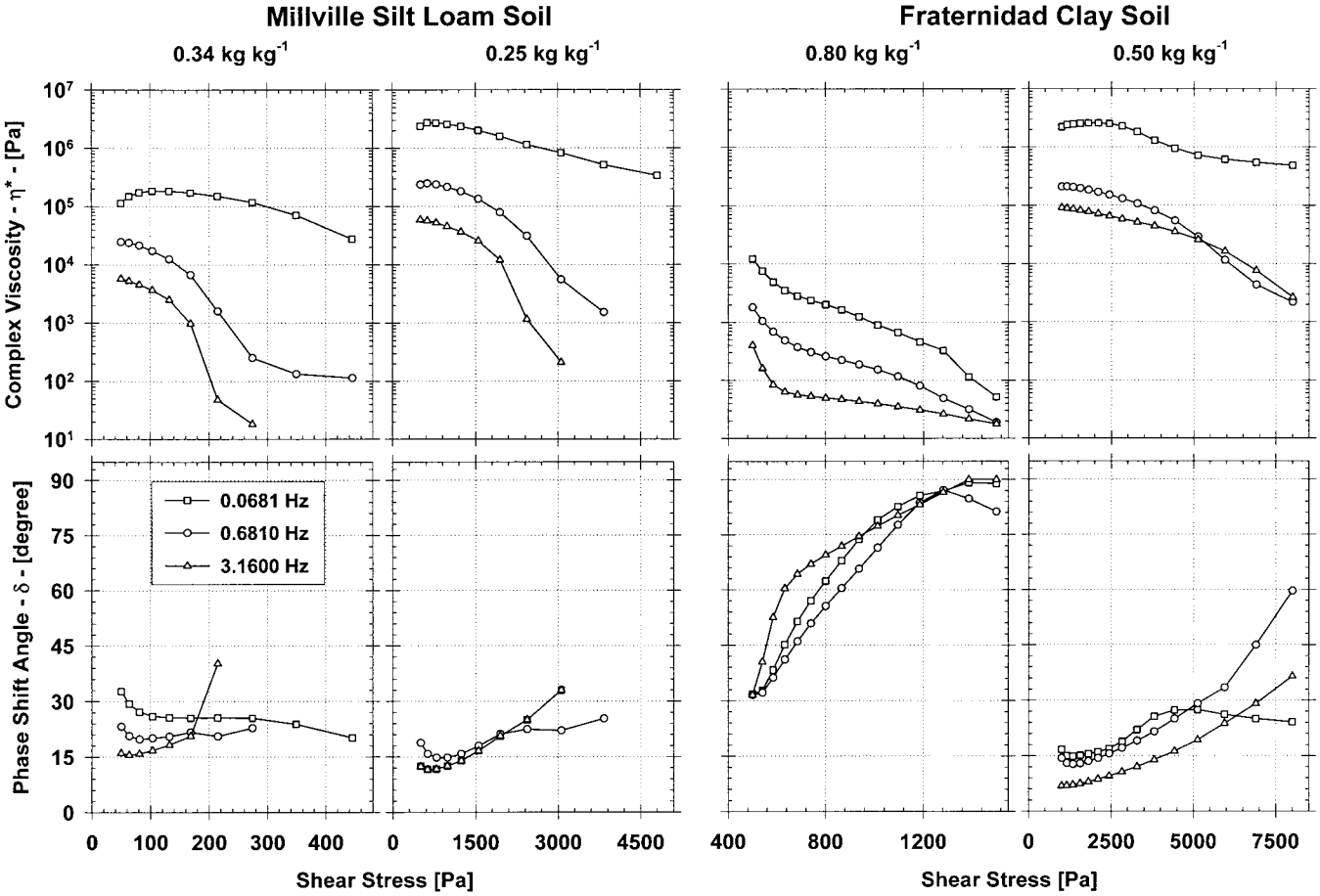

Fig. 11. Summary of viscoelastic properties of Millville silt loam soil and Fraternidad clay soil. Each point in the plots denotes mean of three independent replicates.

(Fig. 11, 12). First, the proportion of viscous deformation (phase shift angle) increases, and second, the overall viscosity decreases. The degree of change in viscosity and phase shift angle are directly related to the heterogeneity of the samples tested. The change in viscosity and phase shift angle with stress is more gradual for the homogeneous clay minerals (kaolinite and Na-montmorillonite) than the natural heterogeneous soils (Millville and Fraternidad). Similarly, the trend is more gradual for the relatively less heterogeneous Fraternidad clay soil than the more heterogeneous Millville silt loam soil.

The Effects of Water Content

At a microscopic scale, an increase in water content increases the spacing between clay domains and quasi-crystals, thereby reducing solid–solid interactions. These, in turn, decrease the complex viscosity and the proportion of elastic strain of the clay water under cyclic load. As a result, increasing water content is accompanied by lower viscosity and higher phase shift angle (decrease in elastic component), for all soils and clays and stress conditions. Other effects of water content and wetting properties of different clay types discussed in the context of viscoplastic properties also apply to the viscoelastic properties.

The Effect of Loading Frequency

The effect of increasing loading frequency (faster tractor speed) is vividly shown in the decreasing viscosity for all soils and clays and stresses (Fig. 11, 12). In contrast, the relative proportion of viscous to elastic deformation (phase shift angle) decreases with frequency for most situations. These observations are related to the differences in loading duration provided by different frequencies. Low frequency testing provides longer loading time, allowing for more viscous dissipation (higher phase shift angle), and vie versa. Comparing viscosity functions of different soils and clays, pure clays have a similar rate of decrease in viscosity with stress at all frequencies. However, natural soil (mixture of different clays and silt) shows a faster rate of decrease of viscosity with stress when loaded at higher frequencies.

Illustrative Examples

For detailed description of soil aggregate coalescence model and resulting evolution of soil pore-size distribution, especially due to wetting and drying cycles, the reader is referred to Ghezzehei and Or (2000) and Or et al. (2000). These models consider viscoplastic deformation of spherical aggregates subjected to steady-state capillary stresses. Because the stresses originate in the

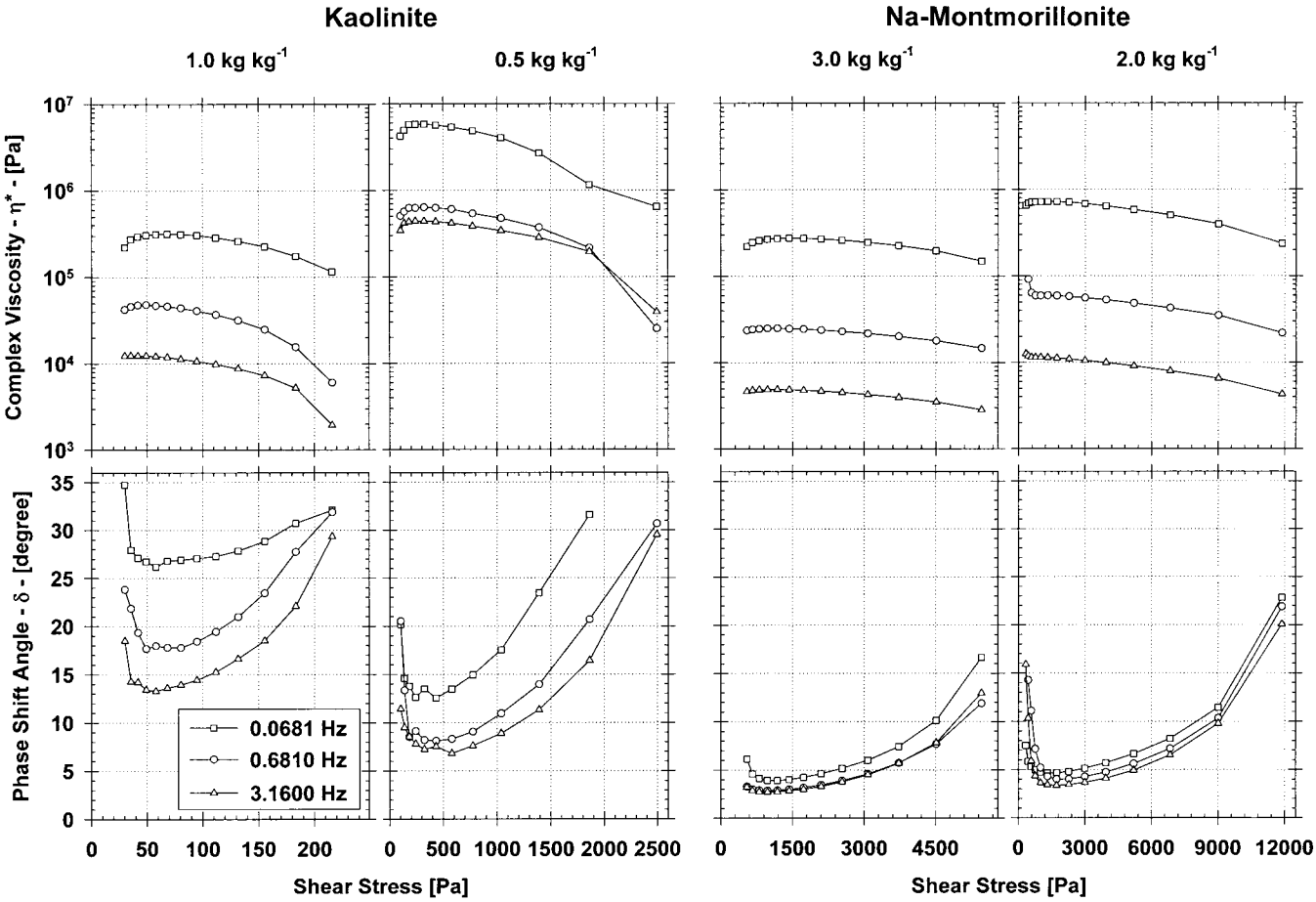

Fig. 12. Summary of viscoelastic properties of kaolinite and Na-montmorillonite clays. Each point in the plots denotes mean of three independent replicates.

vicinity of individual contacts, the process of aggregate coalescence by capillary forces is nondirectional and uniform with depth. In contrast, external forces have a unique direction of maximum impact, and their effect diminishes with depth as stresses are transmitted through overlying aggregates. In general, two forms of external forces, namely, steady and cyclic, are expected. In the following examples, rheological properties of Millville silt loam soil at 0.28 kg kg^{-1} water content will be used along with the simplified models discussed above to demonstrate applications of the rheological properties. These presentations are concerned only with a single contact between identical spherical aggregates. Considerations of different aggregate sizes, interaction between adjacent aggregate pairs, and effect of depth are left for forthcoming work.

Soil Aggregate Deformation under Steady State External Stress

Weight of overlying soil layers (overburden) is an example of steady external forces that exist in all soils. In this example we consider a pair of identical soil aggregates (radius = 1 mm), initially with a very small initial strain ($\varepsilon_o = 0.001$). The line connecting the centers of the aggregates is parallel to the direction of the weight force ($F = 1.63 \times 10^{-4}$ N). The compressive stress (Eq. [11]) acting upon the contacts is shown in Fig. 13a.

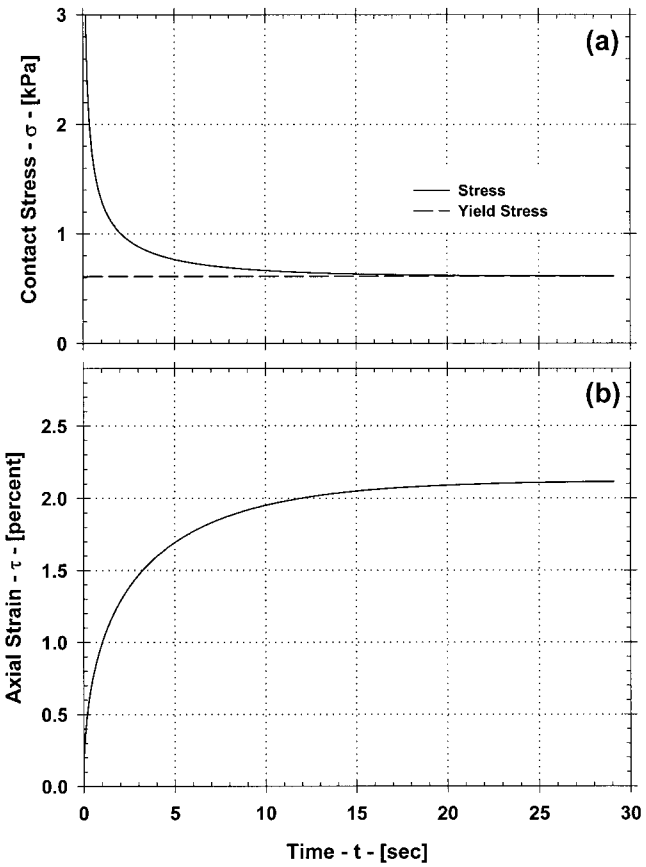

Fig. 13. Stress–strain relationships in aggregate pair model (Millville silt loam soil at 0.28 kg kg^{-1} water content) subjected to steady state stress. (*a*) Applied contact stress and yield stress functions and (*b*) viscoplastic strain response as a function of real time.

Ignoring all the interactions with neighboring aggregates, the strain induced by the stress is given by Eq. [13]. In Fig. 13b, Eq. [13] is evaluated using viscoplastic properties of Millville silt loam soil (0.28 kg kg^{-1} water content).

The Bingham rheological model states that aggregate coalescence occurs only when the applied stress is greater than the yield stress ($\sigma_y = 612$ Pa). Initially, when the interaggregate contact area is nearly zero, the effective stress acting upon the contacts is very high (Fig. 13a) resulting in a rapid rate of aggregate coalescence (slope of Fig. 13b). As the contact area increases with time, the effective stress, hence the rate of aggregate coalescence, decreases. The coalescence ceases when the effective stress equals the yield stress. Further coalescence can be initiated only if the water content is increased (thereby decreasing the yield stress) or the applied load (force) is increased.

Soil Aggregate Deformation under Transient Cyclic Stresses

The most common oscillatory stresses that occur in natural agricultural soils result from passage of farm implements. The force delivered by a tractor can be denoted by a half-cycle sine function Eq. [15]. Qualitatively, the frequency (f) of the sine function is proportional to tractor speed, and the force amplitude (F_o) is proportional to the weight of the tractor.

In the following example we consider a vertically upright aggregate pair (radius = 1 mm), subjected to cyclic force ($F_o = 1.63 \times 10^{-4}$ N). Ignoring all interactions with neighboring aggregates and effect of depth (stress propagation), the strain induced by the passing tractor as a function of time is given by Eq. [18]. For the purpose of comparing different frequencies of stress application that last for different periods, the time (t) is scaled by the frequency as in Eq. [7] and is expressed in units of degrees. The applied oscillatory force Eq. [15] is symmetric about F_o as shown in Fig. 14a. The resulting oscillatory stress, however, is asymmetric (skewed to the right) because it also depends on the increasing strain magnitude. The total strains in a soil aggregate pair (Millville silt loam soil, water content = 0.28 kg kg^{-1}) subjected to two cycles (analogous to front and rear wheel impacts) of slow (0.0681 Hz) and rapid (0.6810 Hz) cycles of stresses are depicted in Fig. 14b.

The viscous strain amplitude occurring at the interaggregate contacts lags behind the stress amplitude by 90°, and the elastic bulging of the aggregates is in phase with the stress curve as shown in Fig. 14b. The magnitudes of the strain components are determined by compound effects of the complex viscosity (η^*) and phase shift angle (δ). In Fig. 14b and 14c, it is indicated that strains at 0.681 Hz are lower than at 0.0681 Hz. Physically, this implies that longer loading time, during slow passage of a tractor, provides enough opportunity time for more viscous straining to occur. The higher phase shift angle (δ) at lower frequency shown in Fig. 11 also suggests a more viscous strain (less elastic) component. In general, the increase in contact area with each additional loading

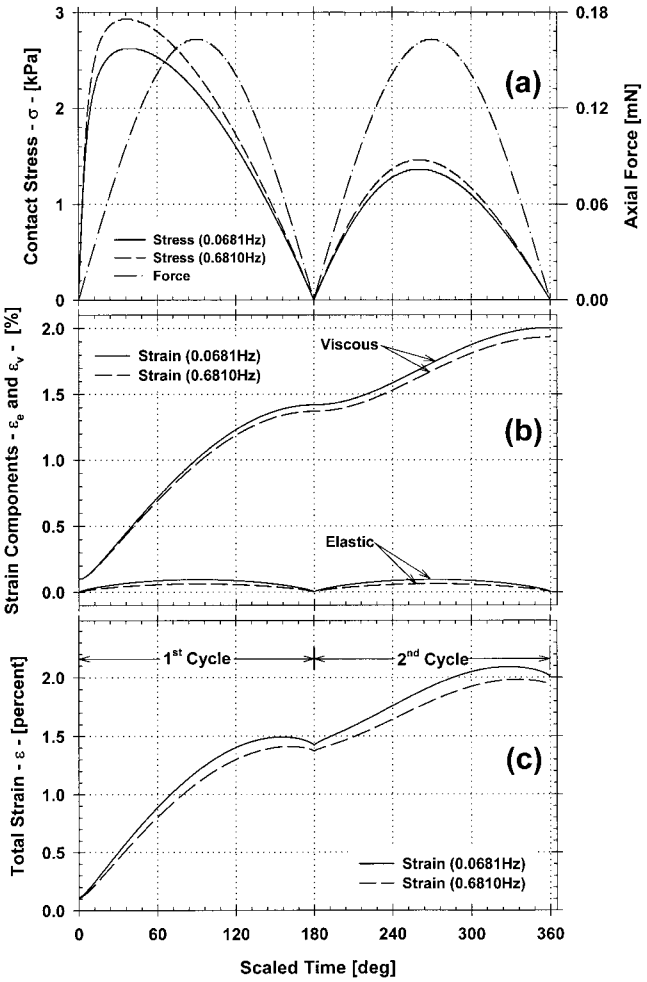

Fig. 14. Stress–strain relationships in aggregate pair model (Millville silt loam soil at 0.28 kg kg^{-1} water content) subjected to two cycles (0.0681and 0.681Hz) of oscillatory stress. (*a*) Applied cyclic force and contact stress, (*b*) elastic and viscous strain components, and (*c*) total strain as functions of scaled time (in degrees).

cycle decreases the effective stress. Consequently, the degree of viscous strain also decreases with the number of cycles. Practically, this implies that the damage incurred by a tractor passing over aggregated soil decreases with the number of passes. Thus, the particular aggregate geometry and soil rheology define the maximum strain level that can be caused by a given stress condition.

SUMMARY AND CONCLUSIONS

This study describes soil rheological properties under stress conditions that mimic actual field conditions. The experimentally determined rheological properties gathered could be used in predicting soil strain and resulting changes in hydraulic properties during compaction of agricultural soil. Soil rheological properties under steady-state and oscillatory stress conditions for different soil and clay types were measured using a rotational rheometer with a parallel plate sensor system. The rationale behind the stress conditions studied (steady and oscillatory) was motivated by stresses commonly occurring in agricultural soils. Steady-state stress occurs in natural soils in two forms: (i) directional overburden of overlying soil, and (ii) omnidirectional capillary forces. Oscillatory stresses are induced by passing farm implements. Measurement results were modeled using simple mechanical analogs (namely; spring, dashpot, and slider) to further assist mathematical analysis of the results. The observed rheological properties and trends were qualitatively explained using soil and clay microstructure and flow processes of clay–water systems.

The main findings and conclusions of this study are as follows:

1. Rheological properties of soils are closely related to microscopic clay structure and flow behavior of clay–water systems. There was qualitative agreement between observed macroscopic rheological properties and expected theoretical and experimental evidence of rheology at microscopic scales.
2. Under steady stress, wet soils and clay minerals exhibit viscoplastic properties characterized by a well-defined yield stress and constant coefficient of plastic viscosity, both of which increase with decreasing water content. These phenomena are related to confinement of liquid water between clay sheets and the resulting decreased ability of water molecules to flow freely, and solid–solid friction.
3. Cyclic or transient loads applied to soil, for example, passage of a tractor, apply stress for only a short duration insufficient for full dissipation of the applied energy, leading to partly recoverable (elastic) strains. This concurrence of viscous and elastic deformations is generally referred to as viscoelasticity.
4. Viscoelastic properties are expressed in compact form using complex viscosity or shear modulus containing both viscous and elastic properties. The relative proportion of each component is provided by the phase shift angle (0° for perfect elastic, 90° for perfect viscous, and intermediate for viscoelastic).
5. Frequency of loading (tractor speed), water content, and stress amplitude are important factors that determine viscoelastic properties. High frequency (corresponding to fast tractor speed) and lower water content result in a higher proportion of elastic deformation and vice versa. High water content and/or high stress amplitude results in lower viscosity of all soils and clays.

The illustrative examples presented, considering single contact between a pair of spherical aggregates, demonstrate the potential usefulness of soil rheological properties for prediction of time-dependent stress–strain relationships, for a given stress condition and water content. Upscaling of the model to multiple contacts involving different soil aggregate geometries (e.g., different sizes) and various packing mechanisms in order to provide quantitative prediction of strain and strain rate of bulk soil are addressed in subsequent work.

ACKNOWLEDGMENTS

The partial funding by USDA/NRI through contract no. 9700814, the U.S.-Israel Binational Agricultural and Research Fund (BARD) through contract no. 2794-96, and the Utah Agricultural Experimental Station (UAES), Utah State University, Logan, UT, are gratefully acknowledged. We thank Victor Snyder, University of Puerto Rico, for providing the Fraternidad clay soil sample. Approved as UAES journal paper no. 7382.

REFERENCES

Abdel-Hady, M., and M. Herrin. 1966. Characteristics of soil-asphalt as a rate process. Proc. ASCE 92(HW1):49–69.

Abramowitz, M., and I.A. Stegun. 1974. Handbook of mathematical functions, with formulas, graphs and mathematical tables. Dover Publ., New York, NY.

Anderslan, O.B., and A.G. Douglas. 1970. Soil deformation rates and activation energies. Geotechnique 20:1–16.

Banfill, P.F.G., and D.R. Kitching. 1991. Use of a controlled stress rheometer to study the yield stress of oilwell cement slurries. p. 373. *In* P.F.G. Banfill (ed.) Rheology of fresh cement and concrete. Chapman and Hall, London.

Ben-Ohoud, M., and H.V. Damme. 1990. The fractal texture of swelling clays and clay–organic aggregates. C R Acad. Sci. Paris 311(II): 665–670.

Carter, D.L., M.M. Mortland, and W.D. Kemper. 1986. Specific surface. p. 413–423. *In* A. Klute (ed.) Methods of soil analysis. Part 1. ASA and SSSA, Madison, WI.

Chenu, C., and D. Tessier. 1995. Low temperature scanning electron microscopy of clay and organic constituents and their relevance to soil microstructure. Scanning Microsc. 9:989–1010.

Collins, K., and A. McGown. 1974. The form and function of microfabric features in a variety of natural soils. Geotechnique 24(2): 223–254.

Day, P.R., and G.G. Holmgren. 1952. Microscopic changes in soil structure during compression. Soil Sci. Soc. Am. Proc. 16:73–77.

Dealy, J.M. 1982. Rheometers for molten plastics: a practical guide to testing and property measurement. Van Nostrand Reinhold, New York.

Dudley, J.G. 1970. Review of collapsing soil. Proc. ASCE 96:925–949.

Eyring, H. 1936. Viscosity, plasticity and diffusion as examples of absolute reaction rates. J. Chem. Phys. 4:283–291.

Fakher, A., C.F.J.P. Jones, and B.G. Clarke. 1999. Yield stress of supersoft clays. J. Geotech. Geoenv. Eng. 125:499–509.

Feda, J. 1989. Interpretation of creep of soils by rate process theory. Geotechnique 39:667–677.

Gee, M.L., P.M. McGuiggan, and J.N. Israelachvili. 1990. Liquid to solidlike transitions of molecularly thin films under shear. J. Chem. Phys. 93:1895–1906.

Ghavami, M., J. Keller, and I.S. Dunn. 1974. Predicting soil density following irrigation. Trans. ASAE 17:166–171.

Ghezzehei, T.A., and D. Or. 2000. Dynamics of soil aggregate coalescence governed by capillary and rheological processes. Water Resour. Res. 36:367–379.

Gierbolini, R.E. 1979. Soil survey of the Ponce area of southern Puerto Rico, USDA-Soil Conservation Service, Washington, DC.

Glastone, S., K.J. Laidler, and H. Eyring. 1941. The theory of rate processes. McGraw-Hill, New York.

Harris, W.L. 1971. The soil compaction process. p. 9–44. *In* K.K. Barnes (ed.) Compaction of agricultural soils. ASAE, St. Joseph, MI.

Hillel, D. 1998. Environmental soil physics. Academic Press, New York.

Horn, R., and T. Baumgartl. 1999. Dynamic properties of soils. p. A19–A51. *In* M.E. Sumner (ed.) Handbook of soil science. CRC Press, Boca Raton, FL.

Hueckel, T.A. 1992. Water–mineral interactions in hygromechanics of clays exposed to environmental loads: a mixture-theory approach. Can. Geotech. J. 29:1071–1086.

Israelachvili, J.N., and G.E. Adams. 1978. Measurement of forces between two mica surfaces in aqueous electrolyte solution. J. Chem. Soc. Faraday Trans. 1 74:975–1001.

Keller, J. 1970. Sprinkler intensity and soil tilth. Trans. ASAE 13:118–125.

Kemper, W.D., 1964. Mobility of water adjacent to mineral surfaces. Soil Sci. Soc. Am. Proc. 25:164–167.

Keren, R., and I. Shainberg. 1984. Colloid properties of clay minerals in saline and sodic solution. p. 32–46. *In* Shainberg and Shalvet (ed.) Soil salinity under irrigation. Springer-Verlag, Berlin.

Koenigs, F.F.R., M.A.M. Mann, and M.Z. Ghazalli. 1976. The mechanical stability of clay soils II: Development of shear strength in clays in dependence of moisture content and suction, desorption of condensed aggregates. Med. Fac. Landbouww. Rijksuniv. Gent 41:117–133.

Koolen, A.J. 1983. Agricultural soil mechanics. Advanced series in agricultural sciences. Springer-Verlag, Berlin.

Kwaad, F.J.P., and H.J. Mücher. 1994. Degradation of soil structure by welding—A micromorphological study. Catena 23:253–268.

Low, P.F. 1976. Viscosity of interlayer water in motmorillonite. Soil Sci. Soc. Am. J. 40:500–504.

Mavko, G., T. Mukerji, and J. Dvorkin. 1998. The rock physics handbook. Cambridge University Press, Cambridge, UK.

McMurdie, J.L. 1963. Some characteristics of the soil deformation process. Soil Sci. Soc. Am. Proc. 27:251–254.

McMurdie, J.L., and P.R. Day. 1958. Compression of soil by isotropic stress. Soil Sci. Soc. Am. Proc. 22:18–22.

Mitchell, J.K. 1956. The fabric of natural clays and its relation to engineering properties. Proc. Highway Res. Board 35:693.

Mitchell, J.K. 1993. Fundamentals of soil behavior. John Wiley and Sons, New York.

Mitchell, J.K., A. Singh, and R.G. Campanella. 1969. Bonding, effective stress, and strength of soils. Proc. ASCE 95(SM5):1219–1246.

Olphen, H.V., and J.J. Fripiat. 1979. Data handbook for clay minerals and other non-metallic minerals. Pergamon Press, Oxford, UK.

Or, D. 1996. Wetting induced soil structural changes: The theory of liquid phase sintering. Water Resour. Res. 32:3041–3049.

Or, D., F.J. Leij, V. Snyder, and T.A. Ghezzehei. 2000. Stochastic model for post-tillage soil pore space evolution. Water Resour. Res. 36:1641–1652.

Or, D., and J.M. Wraith. 1999. Temperature effects on soil bulk dielectric permittivity measured by time domain reflectometry: A physical model. Water Resour. Res. 35:371–384.

Schoen, M., D.J. Diestler, and J.H. Cushman. 1987. Fluids in micropores. I. Structure of a simple classical fluid in a slit-pore. J. Chem. Phys. 87:5464–5476.

Schoen, M., C.L. Rhykerd, D.J. Diestler, and J.H. Cushman. 1989. Shear forces in molecularly thin films. Science 245:1223–1225.

Skipper, N.T., K. Refson, and J.D.C. McConnell. 1991. Computer simulations of interlayer water in 2:1 clays. J. Chem. Phys. 94:7434–7445.

Stepkowska, E. 1990. Aspects of the clay/electrolyte/water system with special reference to the geotechnical properties of clays. Eng. Geol. 28:249–267.

Taylor, D.W. 1948. Fundamentals of soil mechanics. John Wiley and Sons, New York.

Thermo Haake. 1994. Rheometry: Guide to HAAKE Rheometers. Thermo Haake, Karlsruhe, Germany.

Vyalov, S.S. 1986. Rheological fundamentals of soil mechanics. Elsevier, Amsterdam, the Netherlands.